RSC Advances

PAPER

View Article Online
View Journal | View Issue

Check for updates

Cite this: *RSC Adv.*, 2025, **15**, 19500

Synthesis and structural analysis of a ZIF-9/GO composite for green catalytic C–C bond formation and N-formylation: a spectroscopic study†

Lalita Kumari, Rupali Mittal, Mehak Khurana and Satish Kumar Awasthi *

We report a new synthetic approach for a ZIF-9/GO composite material at room temperature and its comprehensive characterization using a variety of techniques, including PXRD, FT-IR, Raman, UV-vis, DRS, TGA, SEM, FE-SEM, EDX, TEM, ICP-MS, XPS, and BET. The material exhibited a moderate surface area and good thermal stability, as indicated by BET and TGA results. DRS revealed a band gap of 3.4 eV, which indicates slight semiconductor nature of the material. The crystalline nature of the ZIF-9/GO composite was confirmed by PXRD. The ZIF-9/GO composite exhibited excellent catalytic efficiency as a heterogeneous catalyst in Knoevenagel condensation and N-formylation, achieving yields of up to 98% under green reaction conditions with a wide range of substrate tolerance. The E-factor (0.10) and atom economy (91.7%) values were very close to ideal green chemistry parameters. *In situ* and UV-vis studies revealed reaction intermediates. The practical utility of this protocol was demonstrated by the gram scale synthesis of the value-added compounds 2-imino-2*H*-1-benzopyran-3-carbonitrile and paracetamol. Single-crystal XRD analysis of three of the compounds confirmed their structural integrity. The catalyst was easily separated *via* filtration and reused for up to six catalytic cycles without significant loss of activity, which is a crucial component of green synthesis, and hot-filtration experiments confirmed its heterogeneity. The probable mechanisms for both reactions are also well presented.

Received 28th March 2025
Accepted 21st May 2025

DOI: 10.1039/d5ra02165k

rsc.li/rsc-advances

Open Access Article. Published on 09 June 2025. Downloaded on 2/11/2026 9:06:38 AM.
This article is licensed under a Creative Commons Attribution-NonCommercial 3.0 Unported Licence.

Introduction

Over the years, heterogeneous catalysis coalesced with sustainable approaches has become as a vital methodology for producing a wide range of chemicals, playing a crucial role in promoting environmentally friendly chemical processes. Compared with homogeneous catalysts, heterogeneous catalysts offer advantages such as ease of product separation, efficient catalyst recycling, and reduced chemical waste generation.[1,2] Furthermore, to address concerns pertaining to the recovery and recyclability of catalytic systems, it is possible to immobilize them on a solid insoluble support. This approach offers several advantages, including improved stability, selectivity, and catalyst activity.[3]

Metal–organic frameworks (MOFs) are crystalline porous materials composed *via* self-assembly of metal atoms and organic ligands through coordination bonds possessing properties such as a large surface area, controllable pore structures, multiple functionalities, high chemical and thermal resistance, and organic-inorganic hybrid nature[4–6] and have been used for many applications such as heterogeneous catalysis,[7,8] energy storage,[9,10] sensors,[11,12] drug delivery[13] and gas separation.[14] One subtype of MOFs is zeolitic imidazolate frameworks (ZIFs), which possess a permanent porous structure and exhibit remarkable stability under thermal and chemical conditions. These properties, such as their high specific area and chemically versatile frameworks, make them highly suitable for use in catalytic applications. Therefore, ZIFs have been widely used for this purpose.[15] Among various ZIFs, ZIF-9 possesses high chemical and thermal stability and includes a network of corner-sharing tetrahedral CoN_4, where the most stable N-donor ligand is present between the Co(II) bond and the benzimidazolate anion.[16,17]

Materials composed of graphene oxide (GO) have demonstrated intriguing physical, optical, and mechanical characteristics. Additionally, they have been successfully used as support materials for organic transformations owing to their substantial specific surface area, high surface-to-volume ratio, thermal stability, and chemical stability.[18–21] GO is a single-layered substance, an oxidized derivative of graphene, and because of

Chemical Biology Laboratory, Department of Chemistry, University of Delhi, Delhi-110007, India. E-mail: satishpna@gmail.com

† Electronic supplementary information (ESI) available: The supporting information includes chemicals and materials; instrumentations; SEM-EDS spectra of ZIF-9/GO; TGA analysis; green chemistry metrics of compound **3c** and **5d**; FESEM and elemental mapping images; BET analysis of ZIF-9 and GO; single-crystal X-ray crystallographic data of compounds **3q**, **5i** and **10o**; UV-vis spectra; post-catalytic characterization; gram-scale synthesis of compounds 7 and **10w**; probable reaction pathway for N-formylation; tables comparing this study with other reported literature; and ^{1}H NMR and ^{13}C NMR spectra. CCDC 2236687 2233222 2341900. For ESI and crystallographic data in CIF or other electronic format see DOI: https://doi.org/10.1039/d5ra02165k

© 2025 The Author(s). Published by the Royal Society of Chemistry

Open Access Article. Published on 09 June 2025. Downloaded on 2/11/2026 9:06:38 AM. This article is licensed under a Creative Commons Attribution-NonCommercial 3.0 Unported Licence.

its intriguing characteristics, including hydrophilicity, high biocompatibility, and cost-effectiveness, graphene oxide is a desirable candidate as a support material.[22]

The combination of ZIF-9 and GO creates a unique class of composites with improved functionality and a large surface area in addition to the inherent properties of both the starting materials. The surface oxygenated groups and defects on GO sheets provide nucleation sites for Co^{2+} ions for the growth of the ZIF-9 framework through coordination bonds.[23] These oxygenated groups and defects stabilizing and anchoring actions on GO may be able to stop ZIF-9 from aggregating and leaking.[24] The use of MOFs or ZIFs with various organic ligands and metals as heterogeneous catalysts for various organic transformations is one of the most diverse fields of research, and from a view of sustainability has attracted considerable attention.[25,26]

The Knoevenagel condensation reaction is the widely used reaction for producing α, β-unsaturated compounds, substituted alkenes and carbon–carbon bonds,[25,27] which are valuable precursors for the synthesis of fine chemicals in the pharmaceuticals industry[28,29] such as nitrendipine, entacapone, lumefantrine and other pharmacological products of calcium channel blockers and antihypertensive, anticancer, antitumor, antimalarial, and antiviral drugs (Fig. 1).[30,31] Knoevenagel condensation can be catalyzed by organic bases,[32] MOFs,[33,34] zeolites,[35] solid-supported materials,[36,37] alkali metal hydroxide and metal oxides,[38–41] and MOFs.[34,42] Interestingly, ZIFs, one of the most promising heterogeneous catalysts, are used in the Knoevenagel condensation reaction.

In addition, the N-formylation of amines is an important reaction. In addition to being useful reagents in Vilsmeier formylation,[43] formamides are important intermediates in the synthesis of pharmaceutically valuable compounds like oxazolidinones,[44] and cancer chemotherapeutic agents.[45] Additionally, formamides have been widely used as Lewis base catalysts in reactions like the synthesis of acid chlorides, hydrosilyation, allylation of carbonyl derivatives,[46,47] isocyanides,[48] and as important amino-protecting groups in peptide synthesis.[49] Chloral,[50] formic acid-DCC,[51] formic acid esters,[52] (chlorodimethoxytriazine) CDMT,[53] ammonium formate,[54] formic acid in sodium formate, and in polyethylene glycol[55,56] are few reported examples of formylating agents.[57] Formic acid (HCOOH), one of many formylating agents, has recently attracted much attention due to its affordability and availability from renewable biomass-derived sources. One of the most recent developments in N-formylation reactions is the catalytic reaction using HCOOH and several different catalysts, such as acidic catalysts ($ZnCl_2$, $AlCl_3$, $NiCl_2$, *etc.*), transition metal/metal oxide catalysts (ZnO, NiO, *etc.*), and inorganic solid oxides (alumina, silica gel, zeolite), oaryloxide-N-heterocyclic carbene ruthenium(II) ([Ru–NHC] complex), molybdate sulfuric acid, sulfated tungstate catalyst, indium nano–cerium oxide, K_3PO_4, heteropoly anion-based ionic liquids (HPAILS), and many others.[58–60] However, these approaches possess several drawbacks, including being expensive and toxic, susceptible to moisture, thermal instability of the reagent/catalyst involved, lack of generality, long reaction time and the need for solvent, anhydrous conditions and elevated temperature.[61,62] According to statistical calculations, amide bonds are present in almost one-fourth of all pharmaceutical medications, including paracetamol, formoterol and phenacetin (Fig. 1).[63]

Thus, in this study, we report ZIF-9/GO as an effective heterogeneous catalyst with high reusability for low-temperature liquid-phase Knoevenagel condensation reaction using malononitrile or ethyl cyanoacetate as the active methylene group and N-formylation of amine using formic acid for the synthesis of benzylidene malononitrile or ethyl-3-cyanoacrylate and formamide derivatives, respectively. The catalytic system works well under greener reaction conditions and demonstrates high substrate applicability, scalability, easy recoverability, and great recyclability.

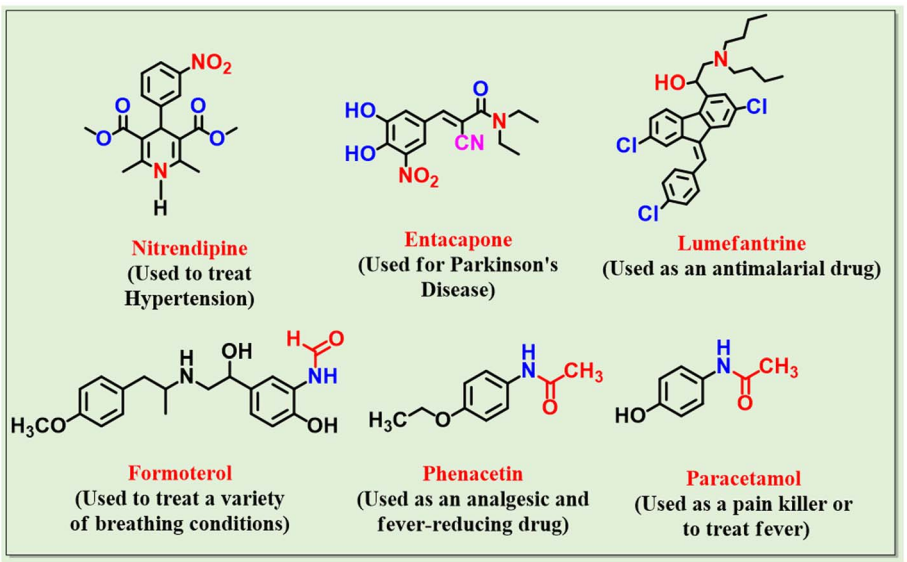

Fig. 1 Knoevenagel condensation-derived (A–C) and amide bond containing (D–F) commercially available therapeutic drugs.

Open Access Article. Published on 09 June 2025. Downloaded on 2/11/2026 9:06:38 AM. This article is licensed under a Creative Commons Attribution-NonCommercial 3.0 Unported Licence.

Experimental section

Catalyst synthesis

Synthesis of ZIF-9. The ZIF-9 synthesis was conducted using a new method. In this method Solution A was prepared by dissolving cobalt nitrate hexahydrate Co $(NO_3)_2 \cdot 6H_2O$ (0.674 g, 2.31 mmol) in 70 mL anhydrous *N*, *N*-dimethylformamide (DMF). Separately, Solution B was prepared by dissolving benzimidazole (3 g, 25.31 mmol) in 35 mL DMF at room temperature. Solution B was then added to solution A, and the mixture was shaken at room temperature until the precipitate was observed (approximately after 1 h). The reaction mixture was then aged for 24 hours at room temperature. The settled precipitate was collected *via* centrifugation at 6000 rpm and subsequently washed three times with ethanol. Finally, the purple ZIF-9 precipitate was dried overnight at 70 °C in an air oven.

Synthesis of graphene oxide (GO). Graphene oxide (GO) was prepared according to Hummer's method with slight modifications.[64,65] 2.5 g of graphite powder and 1.25 g of sodium nitrate ($NaNO_3$) were added to 57.5 mL of concentrated sulfuric acid in an ice bath, and then 7.5 g of $KMnO_4$ was added slowly to the reaction mixture after 10 minutes. After stirring for another 15 minutes, the ice bath was removed, and the reaction mixture was vigorously agitated for 30 minutes at 35 °C. Subsequently, the temperature was increased to 80 °C-85 °C and 115 mL of deionized water was added, and the mixture was agitated for another 15 minutes. The temperature was then reduced to 60 °C with the addition of 350 mL of deionized water followed by the addition of 25 mL of 30% H_2O_2 while stirring. The reaction mixture was then continuously stirred for 2 hours. The precipitates were obtained *via* centrifugation and were then rinsed three times with ethanol, 30% HCl, and water.

Synthesis of ZIF-9/GO composition. Solution A was prepared by mixing Co $(NO_3)_2 \cdot 6H_2O$ (0.674 g, 2.31 mmol) and graphene oxide (0.05 g) in 70 mL dry DMF, followed by sonication till complete dispersion of particles (approximately 30 min). Another solution B was prepared by dissolving benzimidazole (PhIM) (3 g, 25.3 mmol) in 35 mL of DMF. After adding solution B to solution A, the mixture was constantly agitated for 1 hour at room temperature and aged for 24 hours to settle down the precipitates. The precipitates were obtained *via* centrifugation at 6000 rpm and washed with ethanol 3 times. The black precipitate of ZIF-9/GO was then left to dry overnight at 70 °C in an air oven.

General procedure for the ZIF-9/GO catalyzed Knoevenagel condensation. In a 25 mL round-bottom flask, aldehyde (1 mmol), ZIF-9/GO catalyst (10 mg) and ethanol (2 mL) were dissolved and mixed at room temperature. Then, after 5 min, malononitrile (2 mmol) or ethyl cyanoacetate (1 mmol) was added to the reaction mixture. The reaction progress was monitored by thin-layer chromatography. After the completion of the reaction, the catalyst was separated by filtration, and the resulting filtrate was washed at least three times with ethyl acetate and water. The organic layer was concentrated by solvent evaporation, and a product was obtained, which was confirmed by ^{1}H and ^{13}C NMR.

General procedure for the N-formylation of amines using ZIF-9/GO as a catalyst. 1 mmol of amine or aniline was added to 3 mmol of formic acid in an oven-dried 25 mL round bottom-flask consisting of catalyst (10 mg) under neat condition and agitated at room temperature for an appropriate period. Using TLC, the reaction progress was monitored until completion. After completion of the reaction, the catalyst was segregated by filtration, and the filtrate of the reaction was washed at least three times with ethyl acetate and water. The organic layer was washed with sodium bicarbonate solution and dried over anhydrous Na_2SO_4. Finally, the organic layer was concentrated *via* evaporation to obtain the desired product, which was characterized by ^{1}H and ^{13}C NMR and HR-MS analysis.

Results and discussion

In this study, a ZIF-9/GO composite material was synthesized by integrating ZIF-9 and GO materials to achieve their inherent properties as a single material. After successful synthesis, the ZIF-9/GO composite material was subjected to several sophisticated characterizations to gain insight into its structure, composition, and morphology. An illustration of the synthesis procedure of the ZIF-9/GO composite material is provided in Scheme 1.

Evaluation of crystallinity, surface and structural properties, morphology, thermal stability and composition of ZIF-9/GO material

Fig. 2a shows the FT-IR spectra of ZIF-9, GO and ZIF-9/GO. The FT-IR spectrum of ZIF-9 shows peaks at 3020 and 2965 cm^{-1} belonging to aromatic C–H stretching vibrations. The peaks at 1738, 1608 and 1465, 1365, 1235,1277 and 1118 and 745 cm^{-1} correspond to C=N stretching, C=C stretching, C–N stretching, C–C stretching, C–H bending, and C=C/C–H bending, respectively, in the benzimidazole ring, while the peak at 464 cm^{-1} could be correspond to Co–N stretching.[16,66–68] For GO, four characteristic peaks at 3300, 1720, 1615 and 1035 cm^{-1} correspond to the stretching modes of O–H, C=O (carbonyl or carboxylic acid group), C=C (aromatic structure) and C–O (epoxy groups), respectively.[18,22] Some of the GO peaks vanished/reduced in intensity because they were converted to reduced GO during the process. In the FT-IR spectra of ZIF-9/GO, there was a slight shift in some peaks for ZIF-9/GO after the integration of both materials. These attributed peaks of ZIF-9 and GO were noted in the FT-IR spectrum of the composite material ZIF-9/GO, demonstrating that the interaction of the benzimidazole ligand with the cobalt(II) was unaffected by GO immobilization.

Raman spectroscopy is the most significant characterization tool for carbon materials. To understand the crystalline structure and the aberrations, the Raman spectra of GO and ZIF-9/GO were obtained, as shown in Fig. 2b. In the Raman spectrum of GO, two characteristic peaks of carbon materials corresponding to the D band (vibration of sp^3 carbon atoms of disorder in graphitic hexagonal lattice) and G band (vibration of sp^2 carbon atoms in graphitic hexagonal lattice) at 1356 and 1599 cm^{-1}, respectively, were observed.[18,22,69] For the ZIF-9/GO composite material, the peaks were observed at 1357 and

© 2025 The Author(s). Published by the Royal Society of Chemistry

Open Access Article. Published on 09 June 2025. Downloaded on 2/11/2026 9:06:38 AM.
This article is licensed under a Creative Commons Attribution-NonCommercial 3.0 Unported Licence.

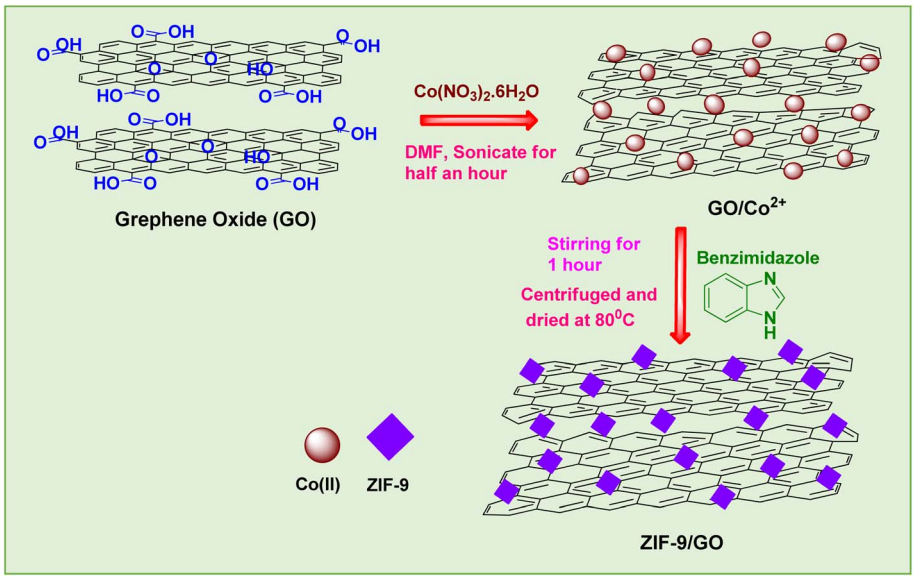

Scheme 1 Graphical illustration of the synthesis of the ZIF-9/GO composite.

1601 cm^{-1}. In composite materials comprising carbon components, the disorder in the structure can be predicted by determining the intensity ratio of the D band and G band (I_D/I_G). In the case of GO and ZIF-9/GO, the I_D/I_G ratios were 0.82 and 0.91, respectively. The higher I_D/I_G ratio value in the case of ZIF-9/GO in comparison to pristine GO is related to the increase in the disorder of the GO structure after the immobilization of ZIF-9 MOF on its surface.[15,18,22]

Brunauer–Emmett–Teller (BET) surface analysis was performed to obtain insights into the textural and surface characteristics of GO, ZIF-9 and ZIF-9/GO *via* nitrogen adsorption–desorption experiment and presented in Fig. 2c. The BET surface analysis of GO and ZIF-9 revealed surface areas of 14.31 and 18.11 $m^2\ g^{-1}$ (Fig. S4†). The pore radius of GO and ZIF-9 were 15.32 and 17.06 Å respectively. The pore volumes of GO and ZIF-9 were 0.032 and 0.019 cc/g, respectively (Fig. S4†). The nitrogen adsorption–desorption isotherm of the ZIF-9/GO

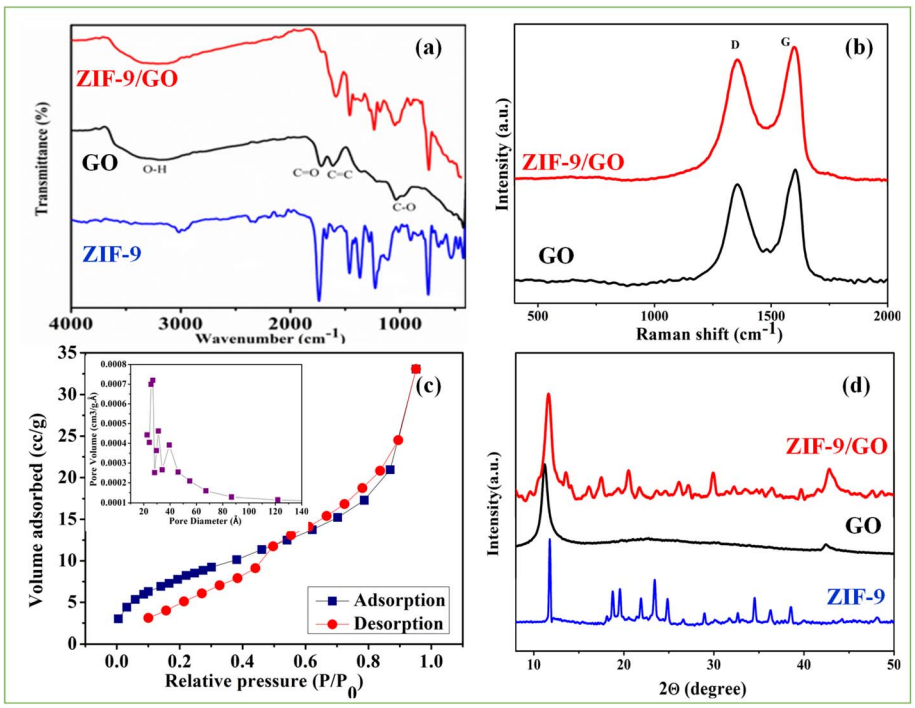

Fig. 2 (a) FT-IR spectra of ZIF-9, GO, and ZIF-9/GO; (b) Raman spectra of GO and ZIF-9/GO; (c) BET surface analysis with the pore size distribution curve of ZIF-9/GO; (d) PXRD patterns of ZIF-9, GO, and ZIF-9/GO.

Open Access Article. Published on 09 June 2025. Downloaded on 2/11/2026 9:06:38 AM. This article is licensed under a Creative Commons Attribution-NonCommercial 3.0 Unported Licence.

composite material displays a type IV isotherm with a hysteresis loop. ZIF-9/GO was found to have a BET surface area of 29.18 m^2 g^{-1}. Using the Barrett–Joyner–Halenda (BJH) method, the pore size and pore volume were 8.04 nm and 0.0507 cm^3 g^{-1}, respectively. The hysteresis loop in nitrogen adsorption–desorption isotherm and the pore size indicate the mesoporous nature of the ZIF-9/GO composite material.

The crystallinity and phase purity of the synthesized materials were studied using their powder XRD patterns, which are presented in Fig. 2d. The XRD patterns of the ZIF-9 and GO samples were in good agreement with the previous literature. The sharp peaks around 2θ = 9.1°, 16.51°, 17.40°, 19.87°, 21.55°, 23.03°, 27.47°, 31.51°, 33.39°, 35.27°, and 37.73° represent the crystalline nature of the ZIF-9 material.[70] For GO, a broad diffraction peak at $2\theta = 11.2°$ (d = 0.79 nm) indicated the presence of (001) plane of the hexagonal system in addition to a minor peak at $2\theta = 42.5°$ (d = 0.21 nm) related to (100) plane related to the hexagonal structure of carbon. The XRD diffraction pattern of ZIF-9/GO composite material displays peaks corresponding to both ZIF-9 and GO, indicating the successful immobilization of ZIF-9 onto the surface of GO.

To evaluate the morphological characteristics of the synthesized samples, SEM and TEM techniques were used. The obtained SEM images for ZIF-9, GO and ZIF-9/GO establish the formation of rhombic dodecahedron-shaped particles, characteristic sheet-like structures, and sheets embedded with rhombic dodecahedron particles, respectively (Fig. 3a–c). Fig. S1† shows the SEM-EDX spectra of ZIF-9/GO, which indicates that elements C, O, N, and Co were found in the sample. The TEM images in Fig. 3d and e show the rhombic dodecahedron and sheet-type morphology of ZIF-9 and GO, respectively. The TEM image of ZIF-9/GO shows the successful growth of ZIF-9 rhombic dodecahedron particles on the sheet-like structure of graphene oxide (Fig. 3f).

Furthermore, to understand the spatial distribution of elements in ZIF-9/GO, FESEM-EDS elemental mapping was performed, as shown in Fig. S3a–S3f†. The images show the uniform dispersion of C, N, O, and Co elements in the ZIF-9/GO composite material.

The thermogravimetric analysis results of ZIF-9, GO and ZIF-9/GO are shown in Fig. S2a.† The ZIF-9 thermogram shows two weight loss stages. The initial minor weight loss of 5% from 100–50 °C was due to the elimination of solvents such as DMF and H_2O present in the Co-ZIF-9 framework. The second sharp weight loss of ∼20% in the range of 560–680 °C was observed along with a weight loss of a total of 46% until 900 °C, indicating the decomposition of the zeolitic imidazolate framework.[17,66,70,71] For GO, a cumulative weight loss of 58% was observed across the three phases. First, at approximately 110 °C, a weight loss of 12% occurred because of the evaporation of adsorbed water molecules. Then, in the temperature range of 160–220 °C, a rapid weight loss of 22% occurred due to the disintegration of groups containing oxygen. Finally, in the temperature range of 220–900 °C, the carbon skeleton of GO undergoes pyrolysis, resulting in a weight loss of 28%.[18] The TGA curve of ZIF-9/GO shows a first weight loss step of 10% up to150 °C because of moisture loss, a second weight loss of 12% up to 212 °C due to the loss of organic solvent, a third weight loss of 16% from 215–400 °C due to degradation of organic moieties, and finally the fourth weight loss of almost 42%, in the temperature range 400–700 °C is observed due to the pyrolysis of the carbon backbone of GO. At last, 20% of the initial weight of ZIF-9/GO remained, indicating the high thermal stability of the material across a broad temperature range. In addition, the cobalt metal content calculated by Inductively Coupled Plasma Mass Spectroscopy (ICP-MS) was approximately 16.52%, which was similar to the TGA result.

X-ray photoelectron spectroscopy (XPS) measurements provide information about the elemental composition,

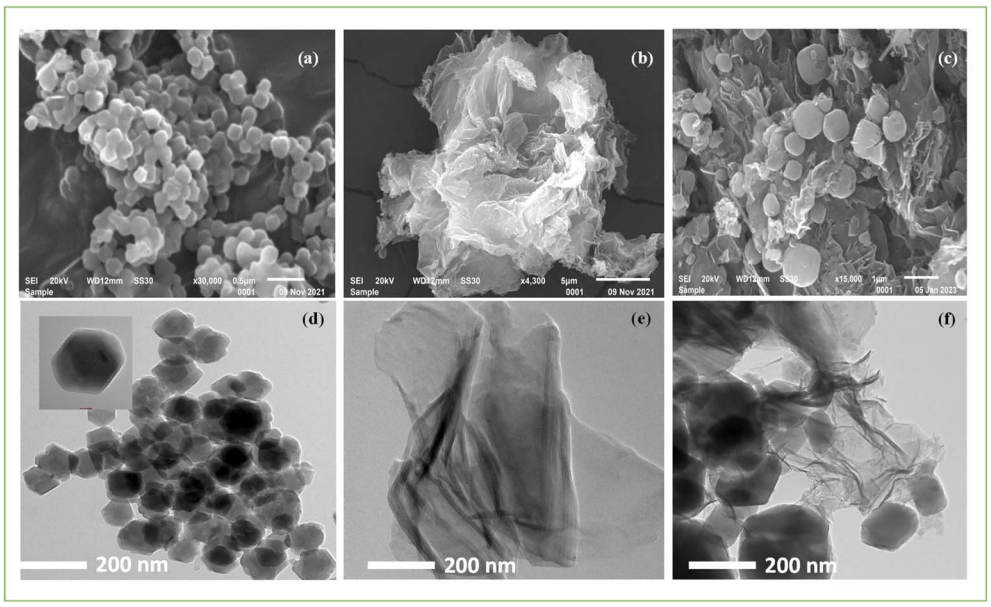

Fig. 3 SEM images of (a) ZIF-9, (b) GO, and (c) ZIF-9/GO, and TEM images of (d) ZIF-9, (e) GO, and (f) ZIF-9/GO.

© 2025 The Author(s). Published by the Royal Society of Chemistry

Open Access Article. Published on 09 June 2025. Downloaded on 2/11/2026 9:06:38 AM. This article is licensed under a Creative Commons Attribution-NonCommercial 3.0 Unported Licence.

chemical environment of the elements, and oxidation states of the metals contained in the ZIF-9/GO sample. The survey spectrum of ZIF-9/GO obtained using XPS is shown in Fig. S2b,† which confirms the existence of O, C, N, and Co elements in the sample, as seen in the elemental mapping and EDS characterizations. The high-resolution spectrum of the O 1s state can be deconvoluted into two bands at 530 eV and 531 eV, as shown in Fig. 4a. The peak at 530 eV is caused by the existence of O–C=O or C–OH groups remaining in the sample, while the peak at 531 eV is indicative of the C–O–C of the epoxy group or the C=O bond of the carboxyl group in the GO sheet.[72] Three peaks can be distinguished in the high-resolution C 1s XPS spectra (Fig. 4b). The peak at 283.4 eV corresponds to the occurrence of adventitious hydrocarbons (C–C/C=C) on the sample's surface. The presence of C–N=C bonds in ZIF-9 and O–C=O bonds from the COOH group of GO, respectively, can be ascribed to the peaks at 285.3 and 286.9 eV. However, in contrast to those of GO, other functional groups (C–C/C–H, C–O, and O–C–O) disappear, which is explained by the chemical interaction between GO and ZIF-9.[27]The deconvoluted N 1s spectrum shows two bands at 397.4 and 399 eV, which is explained by the existence of C–NH/C=N bonds and Co–N bonds, respectively (Fig. 4c). The Co2p XPS spectrum shown in Fig. 4d can be deconvoluted into four peaks. The peaks at 780.50 eV and 795.54 eV can be assigned to the spin–orbit splitting doublets $Co2p_{3/2}$ and $Co2p_{1/2}$ in their Co^{2+} state, respectively, while the peaks at 784.7 eV and 801 eV represent the corresponding satellite that arises from the Co^{2+} ion as well.[3,73,74]

Using the UV-vis absorption spectra, the coordination of ZIF-9 and GO was examined. The UV-vis absorption spectra of GO, ZIF-9, and ZIF-9/GO dispersed in ethanol are shown in Fig. S5.† The GO absorption peaks at 233 or 243 nm and the shoulder peak at approximately 288 nm can be attributed to the $\pi \rightarrow \pi$ transition of the aromatic C=C bond and $n \rightarrow \pi$ transition of the C=O bond, respectively. These peak placements are in good agreement with the findings of numerous other investigations.[22,75] The pristine ZIF-9 absorption spectrum includes a broad absorption band in a range of 400–500 nm and three absorption bands at 243, 272 and 278 nm, corresponding to $\pi \rightarrow \pi^*$ transition,[76] while the UV-vis absorption spectra of ZIF-9/GO composites exhibit a little shift in the absorption bands at approximately 332 nm relative to the pristine ZIF-9 absorption spectrum. This shift in the absorption band may be caused by the charge or energy transfer interaction between the polyaromatic scaffold in GO and ZIF-9, suggesting the possibility of a coordination connection between the two.[24]

The UV-vis diffuse reflectance spectra (DRS), as shown in Fig. 4e, were examined for the coordination geometry and band gap estimation in the ZIF-9/GO composite material. As shown in Fig. 4e, the detection of the absorption band in the range of 480–620 nm with two maxima at 435 and 585 nm can be attributed to tetrahedrally coordinated Co^{2+} ions.[17,73] The absorption band at 255 nm with a shoulder peak at 305 nm is due to π–π^* and n–π^* transitions in graphene oxide. The band gap was calculated using Tauc's relation (Fig. 4f) by plotting the graph between $(\alpha h\nu)$ and energy $(h\nu)^n$, where, α is the absorption coefficient, h is Plank's constant, n is the number for direct or indirect allowed transition, and $h\nu$ is the energy of the photon, found to be 3.42 eV for direct allowed transition, which shows slight semiconductor nature of the material.[77] The increased band gap energy may be due to the presence of insulating graphene oxide in the material.

Catalytic activity studies of ZIF-9/GO in the Knoevenagel condensation reaction

To demonstrate the merits of the ZIF-9/GO composite as a catalytic material in organic synthesis, we applied it to the

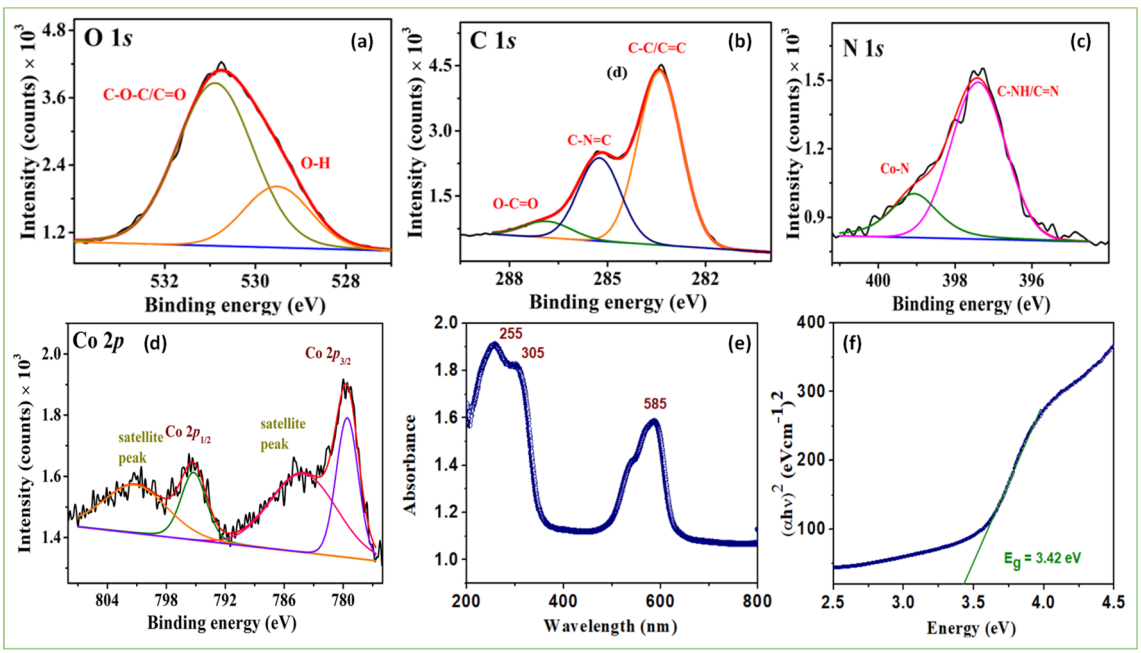

Fig. 4 High-resolution deconvoluted XPS spectra of O 1s (a), C 1s (b), N 1s (c) and Co2p (d). (e) Diffuse reflectance UV-vis spectra and (f) corresponding Tauc plot of ZIF-9/GO.

Open Access Article. Published on 09 June 2025. Downloaded on 2/11/2026 9:06:38 AM. This article is licensed under a Creative Commons Attribution-NonCommercial 3.0 Unported Licence.

Knoevenagel condensation reaction of diversified aldehyde substrates with malononitrile and ethyl cyanoacetate. Initial optimization studies were conducted by reacting 4-nitrobenzaldehyde **1c** and malononitrile **2** as model substrates. First, the reaction was performed in polar solvents such as ethanol and water without any catalyst, which, after 6 and 12 hours of reaction, resulted in poor yield (30–50%) of the desired product, respectively (Table 1, entries 1 and 2). The catalytic activity of ZIF-9/GO (5 mg) was examined in the absence of a solvent and in the presence of a variety of solvents such as toluene, water, and ethanol at various temperatures (Table 1, entries 3–7). From this optimization, the highest yield of 4-nitrobenzylidine malononitrile **3c** was obtained using ethanol as solvent at room temperature (Table 1, entry 7). Furthermore, the amount of ZIF-9/GO (5–20 mg) was optimized in ethanol solvent at room temperature (Table 1, entries 8–10). There was no increment in the product yield upon increasing the amount of catalyst. It was determined that using ZIF-9/GO (10 mg) as a catalyst in ethanol (2 mL) produced the optimal reaction conditions at room temperature (Table 1, entry 8). Under the optimized conditions, the product4-nitrobenzylidene malononitrile was isolated in 98% yield after 10 min of reaction. The gram scale synthesis of 2-imino-2*H*-1-benzopyran-3-carbonitrile **7** was also carried out with excellent yield, as shown in Scheme S1.†

Substrate scope of the ZIF-9/GO-catalyzed Knoevenagel condensation reaction using benzaldehyde and malononitrile

The substrate scope of the ZIF-9/GO catalysed the Knoevenagel condensation reaction was assessed following the optimisation of reaction conditions. The substrate scope findings are summarised in Table 2. The benzylidene malononitrile derivatives were produced in good to excellent yields (85–98%).

High yields of condensation products were obtained from aromatic aldehydes with electron-withdrawing groups at the ortho/para position than from those substituted with electron-donating groups. The substrate scope was extended to aldehydes with heterocyclic rings, which also produced the condensation product in excellent yields (Table 2, entries **3b**, **3q** and **3t**). Among all heterocycles, the pyridine-substituted aldehyde produced the highest yield (Table 2, entry **3t**). The gram scale synthesis of compound 2-imino-2*H*-1-benzopyran-3-carbonitrile was performed, and the obtained yield was 94% (Table 2, entry 7), as shown in the ESI.† All products were characterized by ^{1}H NMR and ^{13}C NMR (Fig. S9–S30 and S40†).

Substrate scope of the Knoevenagel condensation reaction using benzaldehydes and ethyl cyanoacetate

To extend the scope of the Knoevenagel condensation reaction, the reaction of aldehydes with ethyl cyanoacetate acting as an active methylene compound was also performed under similar circumstances for the reaction (Table 3). However, the reaction of ethyl cyanoacetate **4** with 4-nitrobenzaldehyde **1c** required an elevated temperature (60 °C). The reaction proceeded smoothly, giving an excellent yield of the Knoevenagel condensation product (E)-ethyl 2-cyano-3-(4-nitrophenyl) acrylate **5c** in a slightly longer period than the benzylidene malononitrile derivatives (Table 2).

Table 3 summarizes the substrate scope results of the Knoevenagel condensation reaction between aldehydes and ethyl cyanoacetate derivatives, displaying good to excellent yields (85–96%). Higher yields of condensation products were obtained when aromatic aldehydes were substituted at the ortho/para position with groups that donated electrons compared to those that withdrew electrons. Aldehydes with heterocyclic rings also produced condensation products in excellent yields (Table 3, entries **5a** and **5j**). The high yield of (E)-ethyl 2-cyano-3-(pyridin-4-yl) acrylate (Table 3, entry **5j**) is due to the high reactivity of pyridine towards electrophilic substitution

Table 1 Optimization of the reaction conditions for the synthesis of benzylidene malononitrile derivatives[a]

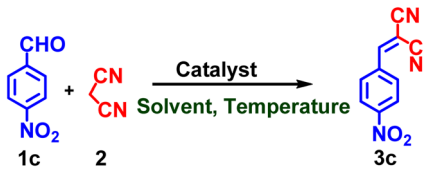

1c 2 3c

Entry	Catalyst amount (mg)	Solvent	Time (h)	Temp. (°C)	Yield [b](%)
1	No catalyst	Ethanol	6	60	50
2	No catalyst	Water	6	80	30
3	5	Solvent-free	4	80	70
4	5	Toluene	4	80	10
5	5	Water	4	80	50
6	5	Ethanol	2	60	80
7	5	Ethanol	2	RT	80
8	**10**	**Ethanol**	**0.10**	**RT**	**98**
9	15	Ethanol	0.10	RT	98
10	20	Ethanol	0.10	RT	96

[a] Reaction conditions: aromatic aldehyde (1 mmol), malononitrile (2 mmol), solvent (2 mL), and catalyst (mg). [b] Isolated yields.

© 2025 The Author(s). Published by the Royal Society of Chemistry

Open Access Article. Published on 09 June 2025. Downloaded on 2/11/2026 9:06:38 AM.
This article is licensed under a Creative Commons Attribution-NonCommercial 3.0 Unported Licence.

Table 2 Substrate scope of the ZIF-9/GO-catalyzed Knoevenagel condensation reaction using malononitrile[a]

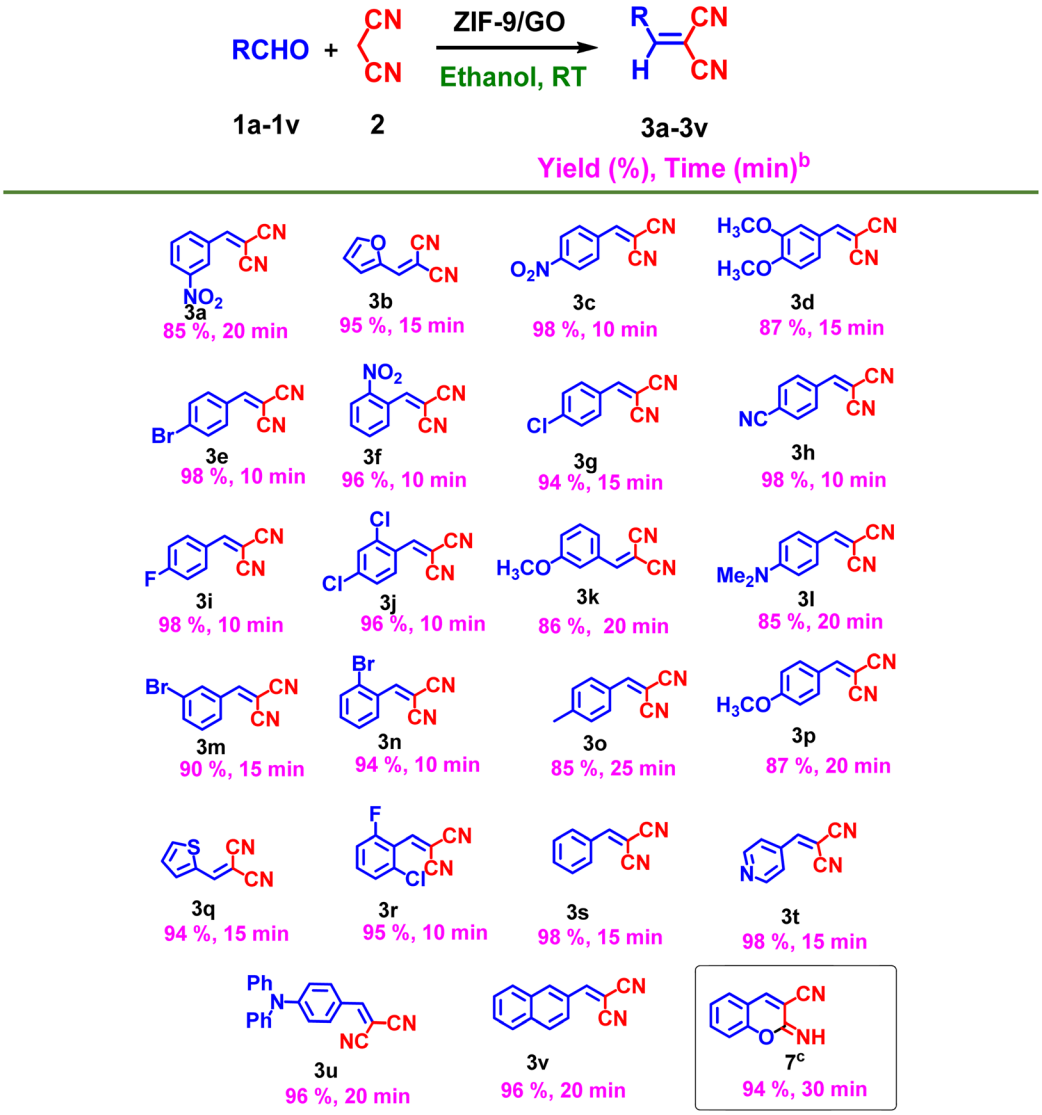

[a] Reaction conditions: aldehyde (1 mmol), malononitrile (2 mmol), catalyst (10 mg), ethanol (2 mL), room temperature, and time (h). [b] Isolated yield. [c] Salicylaldehyde **6** (10 mmol), malononitrile (10 mmol), ZIF-9/GO (100 mg), ethanol (200 mL), and RT.

reaction. All products were characterized by ^{1}H NMR and ^{13}C NMR (Fig. S31–S40†).

Green chemistry parameters

The parameters of green chemistry for the conversion of 4-nitrobenzaldehyde **1c** and 4-fluorobenzaldehyde **1d** to (4-nitrobenzylidine) malononitrile **3c** and (E)-ethyl 2-cyano-3-(4- fluorophenyl) acrylate **5d** were also calculated (Table S1 and S2†). The results of the calculations shown as radar maps in Fig. S6a and S6b† show how closely the values computed using this methodology align with the optimal values of the parameters related to green chemistry. Our green chemistry metrics values show better results than the previously reported ones as shown in Table 4.

Single-crystal X-ray analysis of compound 3q and 5i

The molecular structure of compounds 2-(thiophen-2-ylmethylene) malononitrile **3q** and (E)-ethyl 2-cyano-3-(4-cyanophenyl) acrylate **5i** was confirmed by single-crystal X-ray analysis, which is one of the most thorough methods for determining the chemical structure of compounds. X-ray-grade crystals were formed through the slow solution evaporation growth method in ethanol. The crystal structures (CCDC No. 2236687 and 2233222, respectively) of compounds **3q** and **5i** are shown in Table S3.† They crystallized in a monoclinic cell ($P2_1/c$ space group; Z value = 4) and a triclinic cell ($P\bar{1}$ space group; Z value = 2). The ESI† contains additional single-crystal X-ray crystallographic data for compounds **3q** and **5i** (Table S3†).

© 2025 The Author(s). Published by the Royal Society of Chemistry

Open Access Article. Published on 09 June 2025. Downloaded on 2/11/2026 9:06:38 AM. This article is licensed under a Creative Commons Attribution-NonCommercial 3.0 Unported Licence.

Table 3 Substrate scope of the ZIF-9/GO-catalyzed Knoevenagel condensation from aldehyde to cyano acrylate derivatives[a]

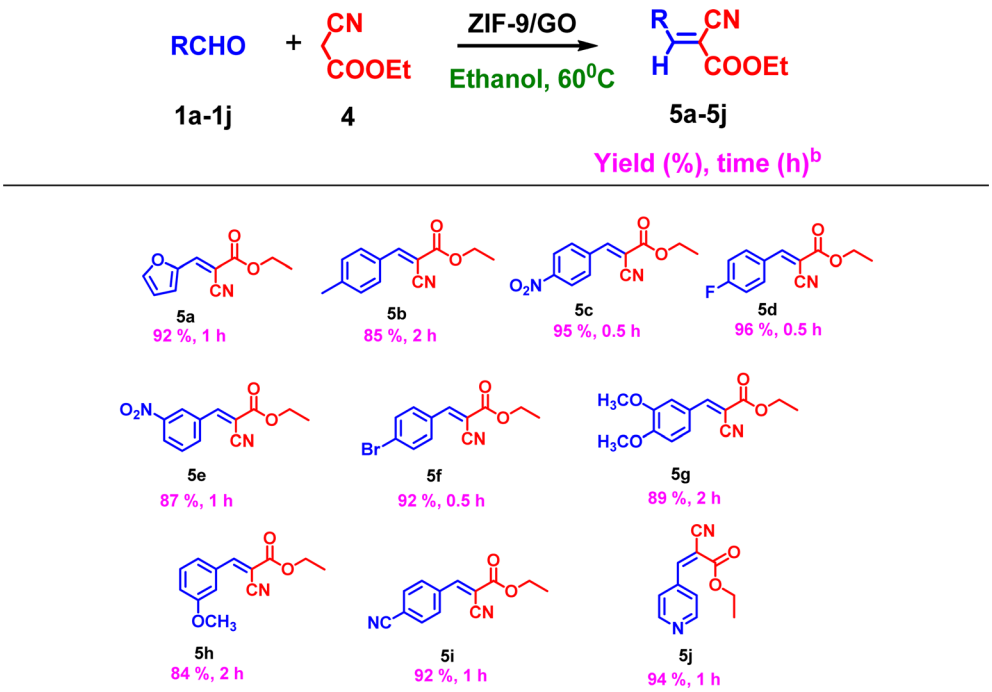

[a] Reaction conditions: aldehyde (1 mmol), ethylcyanoacetate (1 mmol), catalyst (10 mg), 60 °C, time (h), ethanol (2 mL). [b] Isolated yield.

Probable reaction pathway for the Knoevenagel condensation reaction

The possible mechanism for the Knoevenagel condensation reaction between benzaldehyde and the active methylene compound (malononitrile) is illustrated in Fig. 5a. First, the aldehyde group's carbonyl oxygen makes an electrostatic bond with the exposed Co(II) site (Lewis's acid) of the ZIF-9/GO catalyst, turning the carbonyl carbon atom into the electrophilic carbon center (Intermediate I). To produce a carbanion intermediate (II), an uncoordinated benzimidazole (Lewis's base) site adsorbed on ZIF-9/GO acts as a substrate to encourage the deprotonation of methylene. The formed carbanions attack the electrophilic carbonyl carbon. After protonation and dehydration, the addition intermediate (III) can be rapidly transformed into benzylidene malononitrile following the release of the used catalyst.[5,29,39,80]

The UV-visible spectra for the reaction progress from 4-nitrobenzaldehyde (4-NBA) to 4-nitrobenzylidine malononitrile using malononitrile (MN) in the presence of ZIF-9/GO are shown in Fig. 5b. The absorbance peak at 268 nm for 4-nitrobenzaldehyde disappeared and a new absorbance peak at 305 nm for 4-nitrobenzylidine malononitrile appeared, which confirmed the formation of the pure desired product. The absorbance peaks at 272 and 280 nm for the intermediate can be attributed to the malononitrile present in the reaction mixture. All 4-nitrobenzaldehyde was converted into 4-nitrobenzylidine malononitrile within 10 min.

In situ IR study of Knoevenagel condensation

3D *in situ* time-dependent IR spectra of the Knoevenagel condensation reaction were collected to investigate the reaction progress using 4-bromo benzaldehyde and malononitrile as substrates. As shown in Fig. 6, the bands observed in a frequency range of 1550–1750 cm^{-1} were found for the parent benzaldehyde group (Fig. 6a).

Meanwhile, the bands observed after some time in the frequency range of 1350–1550 cm^{-1} were found to be for alkene and nitrile groups present in the product, and the intensity of these bands increased linearly and reached a maximum in 10 min (Fig. 6b). A strong band at 1720 cm^{-1} and a medium band at 1596 cm^{-1} were assigned to the stretching frequency of C=O and C=C of the aromatic group, respectively, and a weak band at 1390 cm^{-1} assigned to C–H bending of aldehyde, which

Table 4 Comparison of green chemistry metrics with other work

Catalysts	*E*-factor	Atom economy (AE)	Process mass intensity (PMI)	Reaction mass efficiency (RME %)	Yield (%)	Reference
NH_2–GCN	0.18	—	1.31	84.50	92	78
$CoFe_2O_4$@SiO_2 @NH_2@BG	0.15	88.10	1.15	87.07	99	79
ZIF-9/GO	0.10	91.7	1.10	90.8	98	This work

© 2025 The Author(s). Published by the Royal Society of Chemistry

Open Access Article. Published on 09 June 2025. Downloaded on 2/11/2026 9:06:38 AM.
This article is licensed under a Creative Commons Attribution-NonCommercial 3.0 Unported Licence.

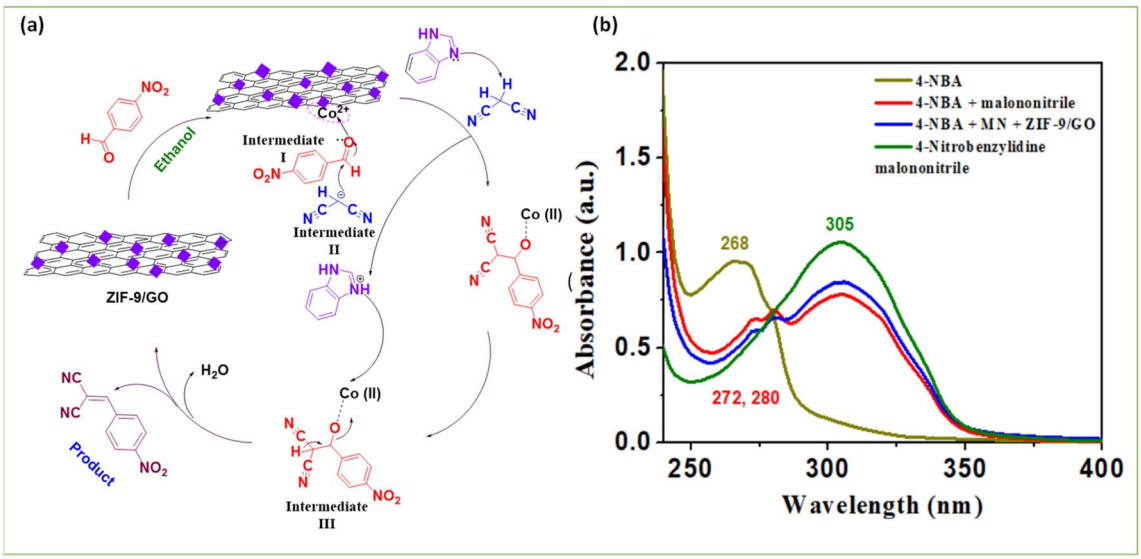

Fig. 5 (a) Probable reaction pathway for the Knoevenagel condensation reaction, and (b) UV-visible spectra for the reaction progress from 4-nitrobenzaldehyde (4-NBA) to 4-nitrobenzylidine malononitrile using malononitrile (MN) in the presence of ZIF-9/GO. The inset shows the percentage conversion of 4-nitrobenzaldehyde (4-NBA) to 4-nitrobenzylidine malononitrile over time.

diminished completely within 10 min, respectively.[81] The other bands at 1520 and 1410 cm^{-1} were assigned to $\nu_{C=C}$ of the aromatic ring and $\nu_{C=C}$ of the alkene. The medium absorption bands at 1150 and 1080 cm^{-1} were attributed to the C–O bond present in the intermediate, which disappeared after reaction completion.

Catalytic activity of ZIF-9/GO towards N-formylation and of amines

The versatility of the catalytic behavior of ZIF-9/GO was examined for the N-formylation of amines with formic acid (**9**) under various reaction conditions (Table 5). Aniline **8r** (1 mmol) and formic acid (3.0 mmol) were used as model substrates for the optimization of reaction parameters, including catalyst quantity, solvent effect, and temperature. Thin-layer chromatography (TLC) was used to carefully monitor the reaction completion.

We began our research by examining the role of the synthesized ZIF-9/GO catalyst in the synthesis of a substituted formamide to optimize the reaction conditions. Without the aid of a catalyst, 1 mmol of aniline **8r** and 3 mmol of formic acid **9** were used as substrates to achieve the above reaction. There was no product formed when the reaction was conducted without

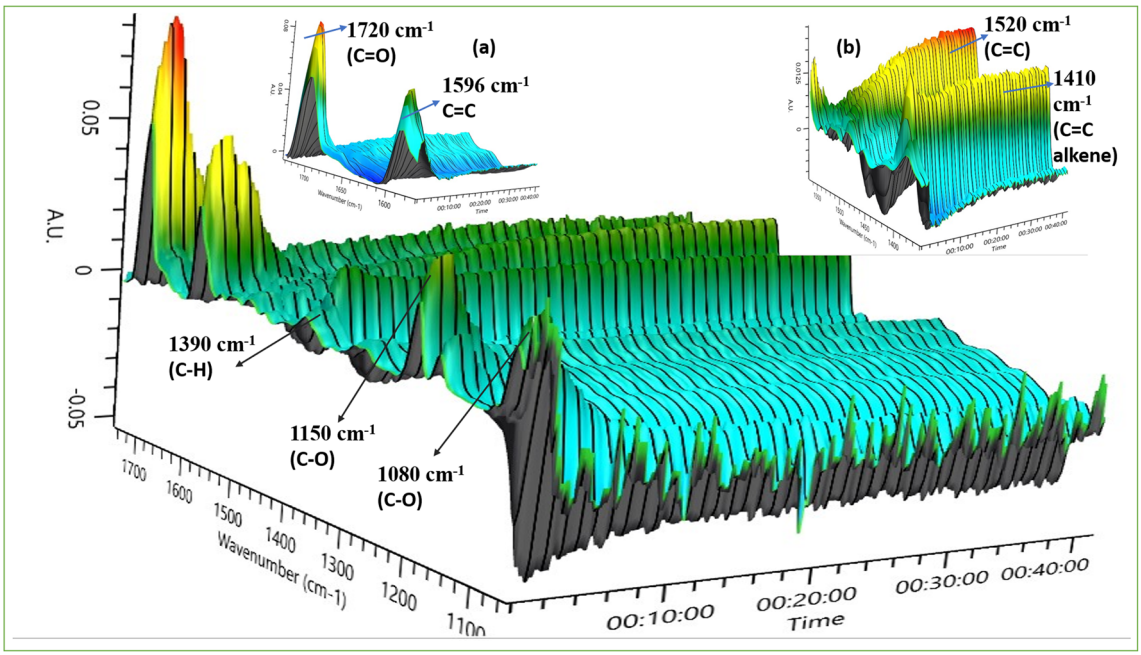

Fig. 6 3D spectra of *in situ* time-dependent infra-red for the Knoevenagel condensation reaction. Zoomed *in situ* IR spectra of the absorption bands of the (a) reactant and (b) product.

Open Access Article. Published on 09 June 2025. Downloaded on 2/11/2026 9:06:38 AM. This article is licensed under a Creative Commons Attribution-NonCommercial 3.0 Unported Licence.

a catalyst, demonstrating the need for a catalyst to produce the required formamide product. The selected reaction of aniline and formic acid was then conducted by varying the amount of synthesized ZIF-9/GO catalyst to examine the impact of catalyst quantity on the reaction. When the catalyst loading was increased from 5 mg to 20 mg, a striking increase in the yield with a decrease in time for the synthesis of the formamide **10r** product was observed, which can be explained by the increase in the number of catalytically active sites. When the amount of catalyst was further increased, no discernible drop in the reaction time or increment in the yield of the desired product was noticed. To achieve the highest conversion rate and for subsequent trials, 10 mg of catalyst was fixed.

Furthermore, the formation of the product was significantly influenced by the solvent used. By modifying the polarity, solubility, and dispersion of the catalyst, solvents have the power to change the reaction environment. Hence, to examine the effect of solvent in formamide synthesis, we optimized the reaction with different types of solvents, including water, ethanol, and toluene, as well as solvent-free conditions. No such increase in the product's % yield was noticed. However, the above experiments show that a polar solvent such as ethanol somehow increases the yield of the desired product compared to a non-polar solvent such as toluene. The highest yield of acetanilide was obtained under solvent-free conditions. Despite this, the reaction proceeded smoothly when water was used as the solvent, but a longer time was required to complete the reaction.

Substrate scope of the synthesis of formamide derivatives using ZIF-9/GO as a catalyst

The synthesized ZIF-9/GO catalyst was employed to produce different substituted formamide derivatives by condensation between different aliphatic, aromatic, and heterocyclic amines substituted with electron-withdrawing or electron-donating groups and formic acid under the optimized reaction conditions. Aniline **8a–8w** (1.0 mmol), formic acid **9** (3.0 mmol), and catalyst (10 mg) were placed in an RB and allowed to react for a predetermined amount of time at room temperature without the presence of any solvent. From various substituted aromatic amines and formic acids, a wide variety of useful substituted formamide derivatives can be produced in good to excellent yields. The electronic environment of the substituted amines affects the yield of the desired product and the time taken for the completion of the reaction. Aromatic amines containing ortho- or para-substituted electron-donating groups, such as CH_3 and OCH_3, produced better product yields in slightly less time as compared to meta-substituted amines and amines with electron-withdrawing groups. The formylation reaction of secondary, aliphatic or heterocyclic amines required slightly more time than aromatic primary amines (Table 6, entries **10l**, **10m**, and **10t**) under optimized conditions to produce a good yield of the desired product. Aliphatic and alicyclic amines (Table 6, entry **10u** and **10v**) like morpholine and piperidine were also investigated for the formylation reaction and proved to be effective substrates producing the corresponding products in good to excellent yields. The chemoselectivity of the reaction was also investigated in the formylation of amines in bifunctional compounds (Table 6, entries **10n** and **10t**). The gram-scale synthesis of compound **10w** (Paracetamol) was carried out with excellent yield (Table 6, entry **10w**), with the reaction shown in the ESI.† All compounds were characterized by ^{1}H-NMR, ^{13}C-NMR (Fig. S43–S65†) and HRMS analysis.

Single-crystal X-ray analysis of compound 10o

Single-crystal X-ray analysis of compound N-(2,5-difluorophenyl) formamide **10o** was used to confirm the validity of the present method for the synthesis of formamide derivatives. X-ray-grade crystals were formed through slow solution evaporation growth in ethanol. The crystal structure (CCDC No.

Table 5 Optimization of the reaction conditions for the N-formylation of amines[a]

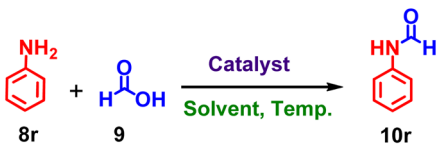

8r 9 10r

Entry	Catalyst amount (mg)	Solvent	Time (h)	Temp. (°C)	Yield [b](%)
1	No catalyst	Ethanol	120	60	N.R.
2	No catalyst	Water	150	80	N.R.
3	5	Ethanol	90	60	50
4	5	Toluene	120	80	10
5	5	Water	120	80	30
6	5	SF	60	60	60
7	5	SF	45	RT	70
8	**10**	**SF**	**5**	**RT**	**98**
9	15	SF	5	RT	98
10	20	SF	10	RT	98

[a] Reaction conditions: aniline (1 mmol), formic acid (3 mmol), solvent (2 mL), and catalyst (mg). [b] Isolated yields.

© 2025 The Author(s). Published by the Royal Society of Chemistry

Open Access Article. Published on 09 June 2025. Downloaded on 2/11/2026 9:06:38 AM. This article is licensed under a Creative Commons Attribution-NonCommercial 3.0 Unported Licence.

2341900) of compound **10o** is presented in Table S3.† It crystallized in a monoclinic cell, *Pn* space group, *Z* value of 2. The ESI† contains additional single-crystal X-ray crystallographic data for compound **10o** (Table S3†).

Recyclability and post-catalytic characterization of the ZIF-9/GO sample

The recyclability of the ZIF-9/GO catalyst was also tested in the Knoevenagel and N-formylation reactions under optimized conditions. After completion of the reaction, the catalyst was extracted from the reaction mixture by filtration. The separated catalyst was rinsed with ethanol and acetone three to four times to remove any organic substances deposited on its surface, followed by drying in an air oven and finally using for further catalytic run under the optimized reaction conditions. The ZIF-9/GO catalyst was reused for six successive runs without a considerable decrease in its catalytic efficiency for both reactions, as shown in Fig. S7a.†

Table 6 Substrate scope of the N-formylation reaction of amines using formic acid[a]

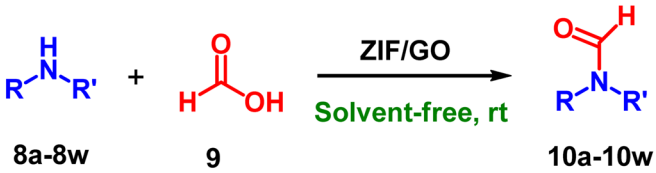

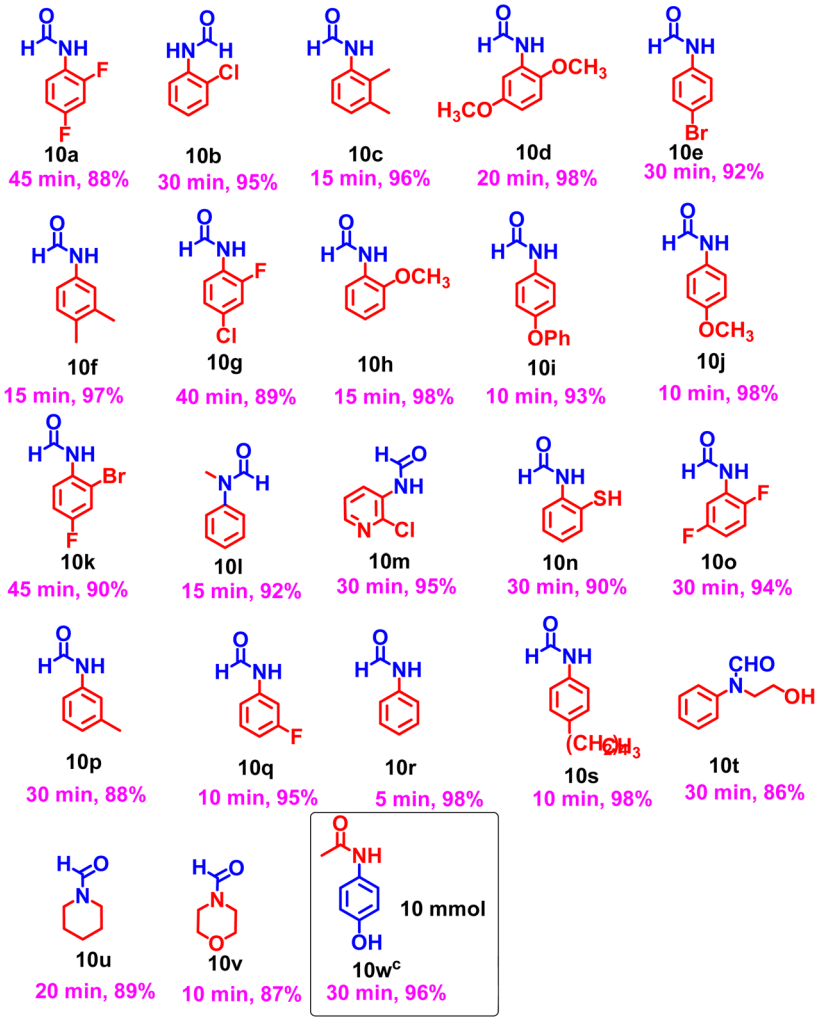

[a] Reaction conditions: amine (1 mmol), formic acid (3 mmol), S·F., ZIF-9/GO (10 mg), and RT. [b] Yield (%). [c] 4-Hydroxy aniline (10 mmol), acetic acid (20 mmol), S·F., ZIF-9/GO (100 mg), and RT.

© 2025 The Author(s). Published by the Royal Society of Chemistry

Open Access Article. Published on 09 June 2025. Downloaded on 2/11/2026 9:06:38 AM. This article is licensed under a Creative Commons Attribution-NonCommercial 3.0 Unported Licence.

The reused ZIF-9/GO was again characterized by SEM, XRD, and FT-IR spectroscopy (Fig. S7b and S7d†) to investigate its stability, morphology, and phase, which showed similar characteristics to those of the original ZIF-9/GO composite material. The observed changes in the XRD peaks of fresh and reused ZIF-9/GO may be due to the presence of reactant or product molecules that may remain adsorbed in the recovered catalyst.

Hot filtration test of the catalyst

Additionally, the "hot filtration method" was used for the synthesis of **3e** as the substrate to study the heterogeneity of ZIF-9/GO. The catalyst was separated from the reaction mixture *via* filtration after 4 minutes, and a 40% conversion of the substrate was observed. Subsequently, the filtrate (without catalyst) was maintained under similar conditions for further reaction. Even after 1 hour, no additional conversion of **3e** was observed (Fig. 7). According to this investigation, the filtrate contained almost no soluble catalytically active species, demonstrating the applicability and heterogeneity of the catalyst.

Probable mechanism for N-formylation of amines using ZIF-9/GO

The exact mechanism of how formylation processes occur using the catalyst remains unclear. However, a putative mechanism in Fig. S8† has been proposed, indicating that the carbonyl group of formic acid is activated by the acidic cobalt ion of the ZIF-9/GO catalyst through a coordination bond, which makes it more electrophilic. The reactive nucleophilic nitrogen atom of the amine group attacks the activated electrophilic carbonyl group to yield the corresponding formylated products.[82,83]

Comparison of catalytic activity of ZIF-9/GO composite material with those reported in previous literature for the Knoevenagel condensation reaction and N-formylation of amine

The importance of this study is shown by comparing the results with previously published work (Tables S4 and S5†). From the comparison table, the present composite material ZIF-9/GO exhibited excellent catalytic activity for the Knoevenagel condensation reaction and synthesis of formamide derivatives with benefits such as easy preparation of the catalyst, mild reaction conditions, high yield of the product, and good recyclability at low catalyst loading.

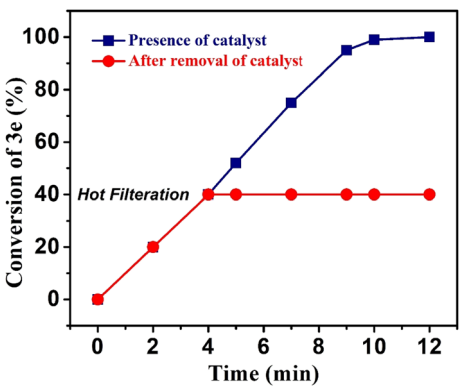

Fig. 7 Hot filtration test of ZIF-9/GO for the synthesis of **3e**.

Conclusions

In conclusion, we report a new synthetic approach for the ZIF-9/GO composite using a straightforward and economical process that combines the conductive and dispersive properties of graphene oxide with the large surface area and stability of ZIF-9. Physiochemical, spectroscopic, and microscopic characterizations confirmed the composition, good crystallinity, thermal stability, structural features, and surface properties of the ZIF-9/GO composite material. ZIF-9/GO was used as a heterogeneous catalyst in Knoevenagel condensation and N-formylation of amines, delivering excellent yields with wide substrate scopes. *In situ* IR study validated the proposed protocol for Knoevenagel condensation. The plausible mechanisms of both reactions were explained in detail. The salient features of this study are outstanding catalytic performance and reusability, easy catalyst recovery, green reaction conditions, low catalyst loading, gram-scale applicability and tolerance to various sensitive substrates in both reactions, highlighting the durability and commercial potential of ZIF-9/GO as a reusable, environmentally benign heterogeneous catalyst.

Data availability

The data supporting the findings of this work are available in the article and its accompanying ESI.† (ESI†) includes Materials and methods,; characterization techniques; SEM-EDX of ZIF-9/GO; TGA analysis and XPS-survey spectrum of ZIF-9/GO; calculation of green chemistry metrics for **3c** and **5d**; FESEM and elemental mapping of ZIF-9/GO; N_2 adsorption–desorption isotherm of GO and ZIF-9; single X-ray crystallographic parameters for **3q**, **5i** and **10o**; UV-visible spectra; radar plot displays green-chemistry metrics of **3c** and **5d**; post-catalytic characterisation; gram-scale synthesis of compound **7**; probable mechanism for both the reactions; comparison table; ^{1}H and ^{13}C NMR chemical shift values; ^{1}H and ^{13}C NMR spectra; FT-IR of **7**; and mass spectra of some compounds.

Conflicts of interest

The authors declare no conflicts of interest.

Acknowledgements

L. K. is appreciative of the senior research fellowship she received from the CSIR in New Delhi, India. S. K. A is thankful to the Institute of Eminence (IoE/Ref.No./IoE/2023–24/12/FRP), University of Delhi, Delhi, India, for financial support. We gratefully acknowledge the University Science Instrumentation Centre (USIC), University of Delhi, Delhi, for analytical data. We are thankful to Sophisticated Analytical Instrument Facility (SAIF)-AIIMS, New Delhi, and IIT-Roorkee, India, for TEM and XPS facility, respectively.

© 2025 The Author(s). Published by the Royal Society of Chemistry

Open Access Article. Published on 09 June 2025. Downloaded on 2/11/2026 9:06:38 AM. This article is licensed under a Creative Commons Attribution-NonCommercial 3.0 Unported Licence.

References

1 R. Mittal and S. K. Awasthi, *ACS Sustain. Chem. Eng.*, 2022, **10**, 1702–1713.
2 F. Monehzadeh and Z. Rafiee, *Appl. Organomet. Chem.*, 2020, **34**, e5631.
3 R. Mittal and S. K. Awasthi, *ChemCatChem*, 2021, **13**, 4799–4813.
4 J. Cong, F. Lei, T. Zhao, H. Liu, J. Wang, M. Lu, Y. Li, H. Xu and J. Gao, *J. Solid State Chem.*, 2017, **256**, 10–13.
5 E. Zare and Z. Rafiee, *Appl. Organomet. Chem.*, 2020, **34**, e5516.
6 A. Das and A. K. Das, *New J. Chem.*, 2023, **47**, 5347–5355.
7 D. Chen, S. Chen, Y. Jiang, S. Xie, H. Quan, L. Hua, X. Luo and L. Guo, *RSC Adv.*, 2017, **7**, 49024–49030.
8 Z. Hasan, J. W. Jun and S. H. Jhung, *Chem. Eng. J.*, 2015, **278**, 265–271.
9 C. Zhang and K. Huang, *Chem. Commun.*, 2017, **53**, 10564–10567.
10 J. Linnemann, L. Taudien, M. Klose and L. Giebeler, *J. Mater. Chem. A*, 2017, **5**, 18420–18428.
11 M. Chhatwal, R. Mittal, R. D. Gupta and S. K. Awasthi, *J. Mater. Chem. C*, 2018, **6**, 12142–12158.
12 S. G. Surya, S. S. Nagarkar, S. K. Ghosh, P. Sonar and V. R. Rao, *Sens. Actuators, B*, 2016, **223**, 114–122.
13 H. Furukawa, N. Ko, Y. B. Go, N. Aratani, S. B. Choi, E. Choi, A. Ö. Yazaydin, R. Q. Snurr, M. O'Keeffe and J. Kim, *Science*, 2010, **329**, 424–428.
14 J. Duan, M. Higuchi, J. Zheng, S.-i. Noro, I.-Y. Chang, K. Hyeon-Deuk, S. Mathew, S. Kusaka, E. Sivaniah and R. Matsuda, *J. Am. Chem. Soc.*, 2017, **139**, 11576–11583.
15 R. Mittal and S. K. Awasthi, *ACS Appl. Nano Mater.*, 2022, **5**, 7831–7840.
16 Q. Li and H. Kim, *Fuel Process. Technol.*, 2012, **100**, 43–48.
17 J. Zakzeski, A. Debczak, P. C. Bruijnincx and B. M. Weckhuysen, *Appl. Catal., A*, 2011, **394**, 79–85.
18 R. Mittal, A. Mishra and S. K. Awasthi, *Synthesis*, 2020, **52**, 591–601.
19 H. J. Shin, K. K. Kim, A. Benayad, S. M. Yoon, H. K. Park, I. S. Jung, M. H. Jin, H. K. Jeong, J. M. Kim and J. Y. Choi, *Adv. Funct. Mater.*, 2009, **19**, 1987–1992.
20 N. R. Wilson, P. A. Pandey, R. Beanland, R. J. Young, I. A. Kinloch, L. Gong, Z. Liu, K. Suenaga, J. P. Rourke and S. J. York, *ACS Nano*, 2009, **3**, 2547–2556.
21 L. Gao, J. R. Guest and N. P. Guisinger, *Nano Lett.*, 2010, **10**, 3512–3516.
22 R. Mittal, A. Kumar and S. K. Awasthi, *RSC Adv.*, 2021, **11**, 11166–11176.
23 Q. Yang, R. Lu, S. Ren, C. Chen, Z. Chen and X. Yang, *Chem. Eng. J.*, 2018, **348**, 202–211.
24 H. Wang, Y. Wang, A. Jia, C. Wang, L. Wu, Y. Yang and Y. Wang, *Catal. Sci. Technol.*, 2017, **7**, 5572–5584.
25 A. Das, D. Chavda, M. Manna and A. K. Das, *New J. Chem.*, 2024, **48**, 18249–18260.
26 A. K. Das, S. Nandy and S. Bhar, *Appl. Organomet. Chem.*, 2021, **35**, e6282.
27 R. Tokala, D. Bora and N. Shankaraiah, *ChemMedChem*, 2022, **17**, e202100736.
28 A. V. Narsaiah and K. Nagaiah, *Synth. Commun.*, 2003, **33**, 3825–3832.
29 H. Tian, S. Liu, Z. Zhang, T. Dang, Y. Lu and S. Liu, *ACS Sustain. Chem. Eng.*, 2021, **9**, 4660–4667.
30 Y. Yang, D. Wang, P. Jiang, W. Gao, R. Cong and T. Yang, *Mol. Catal.*, 2020, **490**, 110914.
31 K. Jain, S. Chaudhuri, K. Pal and K. Das, *New J. Chem.*, 2019, **43**, 1299–1304.
32 D. B. Jackson, D. J. Macquarrie and J. H. Clark, *Spec. Publ.-R. Soc. Chem.*, 2001, **266**, 203–213.
33 R. Cortese and D. Duca, *Phys. Chem. Chem. Phys.*, 2011, **13**, 15995–16004.
34 U. P. Tran, K. K. Le and N. T. Phan, *ACS Catal.*, 2011, **1**, 120–127.
35 M. Opanasenko, A. Dhakshinamoorthy, M. Shamzhy, P. Nachtigall, M. Horáček, H. Garcia and J. Čejka, *Catal. Sci. Technol.*, 2013, **3**, 500–507.
36 V. Calvino-Casilda, R. Martin-Aranda, A. Lopez-Peinado, I. Sobczak and M. Ziolek, *Catal. Today*, 2009, **142**, 278–282.
37 J. Roggenbuck and M. Tiemann, *J. Am. Chem. Soc.*, 2005, **127**, 1096–1097.
38 H. Dabbagh and B. H. Davis, *J. Mol. Catal.*, 1988, **48**, 117–122.
39 H. Teterycz, R. Klimkiewicz and B. Licznerski, *Appl. Catal., A*, 2001, **214**, 243–249.
40 V. N. Panchenko, M. M. Matrosova, J. Jeon, J. W. Jun, M. N. Timofeeva and S. H. Jhung, *J. Catal.*, 2014, **316**, 251–259.
41 N. Liu, Q. Shang, K. Gao, Q. Cheng and Z. Pan, *New J. Chem.*, 2020, **44**, 6384–6393.
42 Z. S. Rozveh, S. P. Aledavoud, S. M. Hosseini, M. Karimi and V. Safarifard, *J. Solid State Chem.*, 2023, **327**, 124270.
43 I. M. Downie, M. J. Earle, H. Heaney and K. F. Shuhaibar, *Tetrahedron*, 1993, **49**, 4015–4034.
44 B. B. Lohray, S. Baskaran, B. S. Rao, B. Y. Reddy and I. N. Rao, *Tetrahedron Lett.*, 1999, **40**, 4855–4856.
45 G. Pettit, M. Kalnins, T. Liu, E. Thomas and K. Parent, *J. Org. Chem.*, 1961, **26**, 2563–2566.
46 S. Kobayashi and K. Nishio, *J. Org. Chem.*, 1994, **59**, 6620–6628.
47 S. Kobayashi, M. Yasuda and I. Hachiya, *Chem. Lett.*, 1996, **25**, 407–408.
48 M.-A. Bonin, D. Giguere and R. Roy, *Tetrahedron*, 2007, **63**, 4912–4917.
49 J. Martinez and J. Laur, *Synthesis*, 1982, **1982**, 979–981.
50 F. Blicke and C.-J. Lu, *J. Am. Chem. Soc.*, 1952, **74**, 3933–3934.
51 M. Waki and J. Meienhofer, *J. Org. Chem.*, 1977, **42**, 2019–2020.
52 H. Yale, *J. Org. Chem.*, 1971, **36**, 3238–3240.
53 L. LD, *Synlett*, 2004, 2570.
54 P. G. Reddy, G. K. Kumar and S. Baskaran, *Tetrahedron Lett.*, 2000, **41**, 9149–9151.
55 G. Brahmachari and S. Laskar, *Tetrahedron Lett.*, 2010, **51**, 2319–2322.

Open Access Article. Published on 09 June 2025. Downloaded on 2/11/2026 9:06:38 AM.
This article is licensed under a Creative Commons Attribution-NonCommercial 3.0 Unported Licence.

56 B. Das, M. Krishnaiah, P. Balasubramanyam, B. Veeranjaneyulu and D. N. Kumar, *Tetrahedron Lett.*, 2008, **49**, 2225–2227.
57 B. Krishnakumar and M. Swaminathan, *J. Mol. Catal. A: Chem.*, 2011, **334**, 98–102.
58 M. Nasrollahzadeh, N. Motahharifar, M. Sajjadi, A. M. Aghbolagh, M. Shokouhimehr and R. S. Varma, *Green Chem.*, 2019, **21**, 5144–5167.
59 M. N. Timofeeva, V. N. Panchenko, I. A. Lukoyanov and S. H. Jhung, *React. Kinet. Mech. Catal.*, 2021, **133**, 355–369.
60 R. Tandon, S. Patil, N. Tandon and P. Kumar, *Lett. Org. Chem.*, 2022, **19**, 616–626.
61 M. Tajbakhsh, H. Alinezhad, M. Nasrollahzadeh and T. A. Kamali, *J. Colloid Interface Sci.*, 2016, **471**, 37–47.
62 M. I. Ansari, M. K. Hussain, N. Yadav, P. K. Gupta and K. Hajela, *Tetrahedron Lett.*, 2012, **53**, 2063–2065.
63 J. K. Yadav, P. Yadav, S. K. Awasthi and A. Agarwal, *RSC Adv.*, 2020, **10**, 41229–41236.
64 W. S. Hummers Jr and R. E. Offeman, *J. Am. Chem. Soc.*, 1958, **80**, 1339.
65 J. H. Lee, J. Jaworski and J. H. Jung, *Nanoscale*, 2013, **5**, 8533–8540.
66 J. Liu, C. Liu and A. Huang, *Int. J. Hydrogen Energy*, 2020, **45**, 703–711.
67 S.-F. Zhang, H. Li, C. Hou, L.-N. Liu, Y. Wang, M.-K. Zhao and C. Liang, *Cellulose*, 2020, **27**, 3287–3300.
68 G. Xiao, W. Chen, Y. Cai, S. Zhang, D. Wang and D. Cai, *Catalysts*, 2022, **12**, 688.
69 Y. Kim and S. Shanmugam, *ACS Appl. Mater. Interfaces*, 2013, **5**, 12197–12204.
70 L. T. Nguyen, K. K. Le, H. X. Truong and N. T. Phan, *Catal. Sci. Technol.*, 2012, **2**, 521–528.
71 Z. Öztürk, J. P. Hofmann, M. Lutz, M. Mazaj, N. Z. Logar and B. M. Weckhuysen, *Eur. J. Inorg. Chem.*, 2015, **2015**, 1625–1630.
72 R. Al-Gaashani, A. Najjar, Y. Zakaria, S. Mansour and M. Atieh, *Ceram. Int.*, 2019, **45**, 14439–14448.
73 S. Yan, S. Ouyang, H. Xu, M. Zhao, X. Zhang and J. Ye, *J. Mater. Chem. A*, 2016, **4**, 15126–15133.
74 Y. Yang, F. Li, W. Li, W. Gao, H. Wen, J. Li, Y. Hu, Y. Luo and R. Li, *Int. J. Hydrogen Energy*, 2017, **42**, 6665–6673.
75 C. Zhang, L. Ren, X. Wang and T. Liu, *J. Phys. Chem. C.*, 2010, **114**, 11435–11440.
76 M. Jahan, Z. Liu and K. P. Loh, *Adv. Funct. Mater.*, 2013, **23**, 5363–5372.
77 N. Sharma, S. Tomar, M. Shkir, R. K. Choubey and A. Singh, *Mater. Today: Proc.*, 2021, **36**, 730–735.
78 K. Kumari, P. Choudhary, D. Sharma and V. Krishnan, *Ind. Eng. Chem. Res.*, 2022, **62**, 158–168.
79 A. Mishra, P. Yadav and S. K. Awasthi, *ACS Org. Inorg. Au*, 2023, **3**, 254–265.
80 E. Rahmati and Z. Rafiee, *J. Porous Mater.*, 2021, **28**, 19–27.
81 J. P. Li, E. M. Kennedy, A. A. Adesina and M. Stockenhuber, *J. Catal.*, 2019, **369**, 157–167.
82 M. Seddighi, F. Shirini and O. Goli-Jolodar, *C. R. Chim.*, 2016, **19**, 1003–1010.
83 R. Chutia and B. Chetia, *New J. Chem.*, 2018, **42**, 15200–15206.

© 2025 The Author(s). Published by the Royal Society of Chemistry